ISSN 1674-1056
http://cpb.iphy.ac.cn
http://iopscience.iop.org/cpb
中国物理 B
Chinese Physics
中国物理 Chinese Physics B

Enhancement of thermoelectric properties of $SrTiO_3$/LaNb-$SrTiO_3$ composite by different doping levels

Ke-Xian Wang(王柯鲜), Jun Wang(王俊), Yan Li(李艳), Tao Zou(邹涛), Xiao-Huan Wang(王晓欢), Jian-Bo Li(李建波), Zheng Cao(曹正), Wen-Jing Shi(师文静), Xinba Yaer(新巴雅尔)
Citation: Chin. Phys. B . 2018, 27(4): 048401. **doi:** 10.1088/1674-1056/27/4/048401

Journal homepage: http://cpb.iphy.ac.cn; http://iopscience.iop.org/cpb

What follows is a list of articles you may be interested in

Band engineering and precipitation enhance thermoelectric performance of SnTe with Zn-doping

Zhiyu Chen(陈志禹), Ruifeng Wang(王瑞峰), Guoyu Wang(王国玉), Xiaoyuan Zhou(周小元), Zhengshang Wang(王正上), Cong Yin(尹聪), Qing Hu(胡庆), Binqiang Zhou(周斌强), Jun Tang(唐军), Ran Ang(昂然)
Chin. Phys. B . 2018, 27(4): 047202. **doi:** 10.1088/1674-1056/27/4/047202

Effects of Mn substitution on thermoelectric properties of $CuIn_{1-x}Mn_xTe_2$

Pengfei Luo(罗鹏飞), Li You(游理), Jiong Yang(杨炯), Juanjuan Xing(邢娟娟), Jiye Zhang(张继业), Chenyang Wang(王晨阳), Xinluo Zhao(赵新洛), Jun Luo(骆军), Wenqing Zhang(张文清)
Chin. Phys. B . 2017, 26(9): 097201. **doi:** 10.1088/1674-1056/26/9/097201

Improved thermoelectric performance in p-type $Bi_{0.48}Sb_{1.52}Te_3$ bulk material by adding $MnSb_2Se_4$

Binglei Cao(曹丙垒), Jikang Jian(简基康), Binghui Ge(葛炳辉), Shanming Li(李善明), Hao Wang(王浩), Jiao Liu(刘骄), Huaizhou Zhao(赵怀周)
Chin. Phys. B . 2017, 26(1): 017202. **doi:** 10.1088/1674-1056/26/1/017202

Charge and spin-dependent thermal efficiency of polythiophene molecular junction in presence of dephasing

Z. Golsanamlou, M. Bagheri Tagani, H. Rahimpour Soleimani
Chin. Phys. B . 2015, 24(10): 108402. **doi:** 10.1088/1674-1056/24/10/108402

Thermoelectric properties of $Sr_{0.61}Ba_{0.39}Nb_2O_{6-\delta}$ ceramics in different oxygen-reduction conditions

Li Yi, Liu Jian, Wang Chun-Lei, Su Wen-Bin, Zhu Yuan-Hu, Li Ji-Chao, Mei Liang-Mo
Chin. Phys. B . 2015, 24(4): 047201. **doi:** 10.1088/1674-1056/24/4/047201

SPECIAL TOPIC — Recent advances in thermoelectric materials and devices

Enhancement of thermoelectric properties of $SrTiO_3$/LaNb–$SrTiO_3$ composite by different doping levels*

Ke-Xian Wang(王柯鲜)[1], Jun Wang(王俊)[1,†], Yan Li(李艳)[2], Tao Zou(邹涛)[3], Xiao-Huan Wang(王晓欢)[1], Jian-Bo Li(李建波)[1], Zheng Cao(曹正)[1], Wen-Jing Shi(师文静)[1], and Xinba Yaer(新巴雅尔)[1,‡]

[1] *School of Materials Science and Engineering, Inner Mongolia University of Technology, Hohhot* 010051, *Inner Mongolia Autonomous Region, China*
[2] *School of Chemical Engineering, Kang Ba Shi Qu, Ordos, Ordos Institute of Technology, Ordos* 017000, *Inner Mongolia Autonomous Region, China*
[3] *Beijing Center for Physical & Chemical Analysis, No. 27 Xi Sanhuan Road, Haidian District, Beijing* 100089, *China*

(Received 21 December 2017; revised manuscript received 28 January 2018; published online 10 March 2018)

Strontium titanate (STO) is an n-type oxide thermoelectric material, which has shown great prospects in recent years. The doping of La and Nb into STO can improve its power factor, whereas its thermal conductivity is still very high. Thus, in order to obtain a high thermoelectric figure-of-merit zT, it is very important to reduce its thermal conductivity. In this paper, using a combination of a hydrothermal method and a high-efficiency sintering method, we succeed in preparing a composite of pure STO and LaNb-doped STO, which simultaneously realizes lower thermal conductivity and higher Seebeck coefficient, therefore, the thermoelectric properties of STO are significantly improved. In the $SrTiO_3$/LaNb–$SrTiO_3$ bulk samples, the lowest thermal conductivity is 2.57 $W\cdot m^{-1}\cdot K^{-1}$ and the highest zT is 0.35 at 1000 K for the STO/La10Nb20–STO sample.

Keywords: thermoelectric materials, $SrTiO_3$/LaNb–$SrTiO_3$ composite, hydrothermal method, strontium titanate

PACS: 84.60.Rb, 72.15.Jf, 77.84.Cg, 81.20.–n **DOI:** 10.1088/1674-1056/27/4/048401

1. Introduction

Owing to serious energy consumption and environmental pollution, efficient energy conversion is urgently needed. The thermoelectric material can directly convert heat into electrical energy. By using a small volume thermoelectric device, a portion of the waste heat can be transformed into useful energy with low noise and no pollution. The thermoelectric conversion efficiency is characterized by the dimensionless value $zT = S^2\sigma T/\kappa$, where S, σ, T, and κ are the Seebeck coefficient, electrical conductivity, absolute temperature, and thermal conductivity, respectively. High-performance thermoelectric material requires a high Seebeck coefficient, high electrical conductivity as well as low thermal conductivity.

The lower conversion efficiency of the thermoelectric material always restricts the large-scale application of thermoelectric devices. There have been many studies on alloys to attempt to increase their conversion efficiency in recent years. The carrier and phonon transport properties are optimized by doping,[1–3] microstructure control,[4–7] band engineering,[4,5,8–10] and other methods,[11–15] which can also improve the thermoelectric properties. The studies of oxide thermoelectric materials have lagged behind alloy development because of their high thermal conductivity or low electrical conductivity. As said above, $SrTiO_3$ is a typical n-type oxide thermoelectric material with low toxicity, high thermal stability, and large Seebeck coefficient, therefore it has great prospects in future applications. A lot of thermoelectric studies have been carried out on $SrTiO_3$ by composite materials,[16–18] doping,[19,20] and producing defects.[21,22] Upon doping, the Seebeck coefficient and electrical conductivity appear to be relatively high, whereas the thermal conductivity is still high, resulting in an inconspicuous improvement of the zT value.

In this work, according to the study of the idea of the core-shell structure of thermoelectric material,[6,23–28] we prepare the STO/LaNb–STO composite materials. Because the two components of pure $SrTiO_3$ and LaNb–$SrTiO_3$ in this composite have similar energy band structures, the prepared composite could have several merits. First, the high Seebeck coefficient can be kept unchanged. Second, increasing the number of interfaces can reduce the thermal conductivity. Third, electrical conductivity can also keep a high value by heavy electron doping. However, there have been few reports on $SrTiO_3$/LaNb–$SrTiO_3$ composite materials so far.

*Project supported by the National Natural Science Foundation of China (Grant Nos. 61751404, 51702168, and 51665042), the Fund from the State Key Laboratory of New Ceramic and Fine Processing (Tsinghua University), China (Grant No. KF201608), the Fund from the Guangxi Key Laboratory of Information Materials, Guilin University of Electronic Technology, China (Grant No. 151004-K), and the Natural Science Foundation of Inner Mongolia Autonomous Region, China (Grant Nos. 2016BS0507 and 2015MS0509).

†Corresponding author. E-mail: wangjun@imut.edu.cn
‡Corresponding author. E-mail: shinbayaer@imut.edu.cn

© 2018 Chinese Physical Society and IOP Publishing Ltd

2. Experimental method

2.1. Sample preparation

The size and quality of starting powders are important for achieving high thermoelectric performance. The hydrothermal method is suitable to synthesizing high quality nano-powder. In this study, a hydrothermal method (HTS) and a sintering method[29] are combined to prepare the STO/LaNb–STO composite materials. Pure STO powder was prepared by the hydrothermal method. La and Nb-doped STO precursor was prepared by using ethylene glycol, Ti $(OBu)_4$, $NbCl_5$, $Sr(NO_3)_2$, $La(NO_3)_2 \cdot 6H_2O$, and NaOH. After that, the prepared pure $SrTiO_3$ powder was placed in this solution. The forming solution was placed in a stainless steel reactor and heated at 180 °C for 24 h, followed by well mixing through an ultrasonic wave. The obtained powders were compacted into a disk by die pressing at 5 MPa and then cold isostatic pressing (CIP) under 20 MPa into the disk. The disk-shape samples were embedded in carbon powders in a corundum crucible, and they were placed into a muffle furnace at 1300 °C for 5-h sintering. After that, the sintered disk samples were sufficiently polished to obtain STO/LaNb–STO composites. The sample preparation process is shown in Fig. 1. Four different composites are STO/La5Nb5–STO (pure $SrTiO_3$: 5-mol% La and 5-mol% Nb doped $SrTiO_3$), STO/La5Nb10–STO, STO/La10Nb10–STO, and STO/La10Nb20–STO, respectively, where the mole ratio of pure $SrTiO_3$ and LaNb–$SrTiO_3$ is 1:1 in all composites.

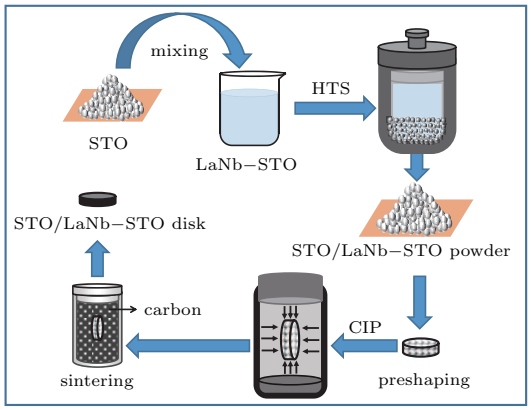


Fig. 1. (color online) Schematic diagram of preparation method.

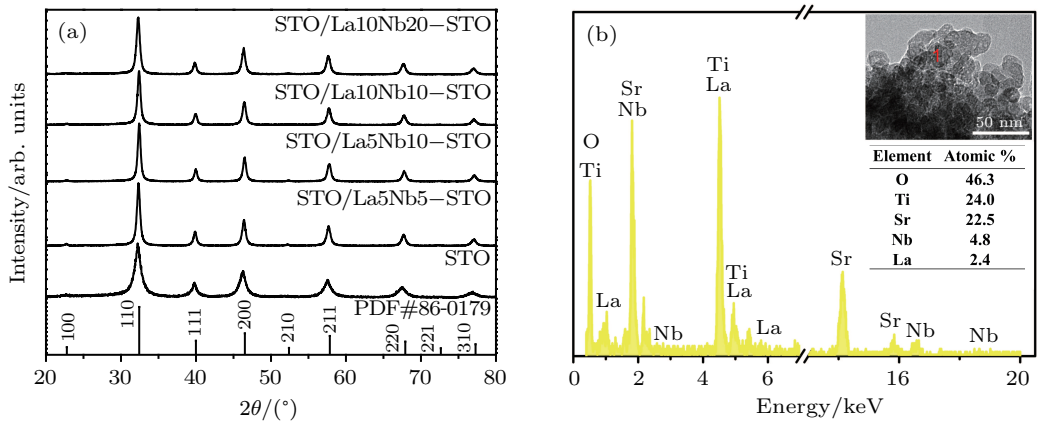
2.2. Sample characterization

The compositions and microstructures of the samples were characterized by scanning electron microscopy (SEM, Hitachi SU8010), x-ray diffraction (XRD, Rigaku D/Max-2500) and transmission electron microscopy (TEM, FEI Tecnai G2 F20), respectively. Ratios of Sr, La, Ti, and Nb in the sample were obtained from energy dispersive spectrometers equipped with SEM (EDS/SEM) and TEM (EDS/TEM). The electrical conductivity and the Seebeck coefficient were measured in a helium atmosphere from 300 K to 1100 K by using the Linseis LSR-3. The thermal conductivity (κ) was calculated from the equation $\kappa = DC_p\rho$, where the thermal diffusivity (D) was measured by the laser flash method using the Netzsch LFA 457, the specific heat (C_p) was measured by a differential scanning calorimeter using a Netzsch DSC STA 449F3, and the density (ρ) was measured by the Archimedes method.

3. Results and discussion

3.1. Microstructure analysis

Figure 2(a) shows the x-ray diffraction patterns of the STO/LaNb–STO composite powder samples. The diffraction peaks of powders match with pure cubic perovskite structure, and the widening of the peaks indicates that the particle size of the powder is small. The peaks of doped samples are a little deviated from that of the pure one because the ion radii of La and Nb differ from those of Sr and Ti.[30] The deviation depends on the La and Nb doping concentrations. In addition, from the analysis of the EDS/TEM for STO/La10Nb20STO powders (Fig. 2(b)), the presence of La and Nb besides the Sr and Ti peaks is also confirmed. These indicate that La and Nb are actually doped into the $SrTiO_3$ crystal lattice. The TEM image (Fig. 2(c)) of STO/La10Nb20 powder illustrates that the powder is irregularly flaky-shaped and the sizes are approximately 15 nm–25 nm. The high resolution image in Fig. 2(d) reveals that the distance between the adjacent lattice stripes is 0.27 nm, that is consistent with the typical (110) plane of $SrTiO_3$, which is a further proof of the cubic perovskite structure of the obtained $SrTiO_3$ powder.



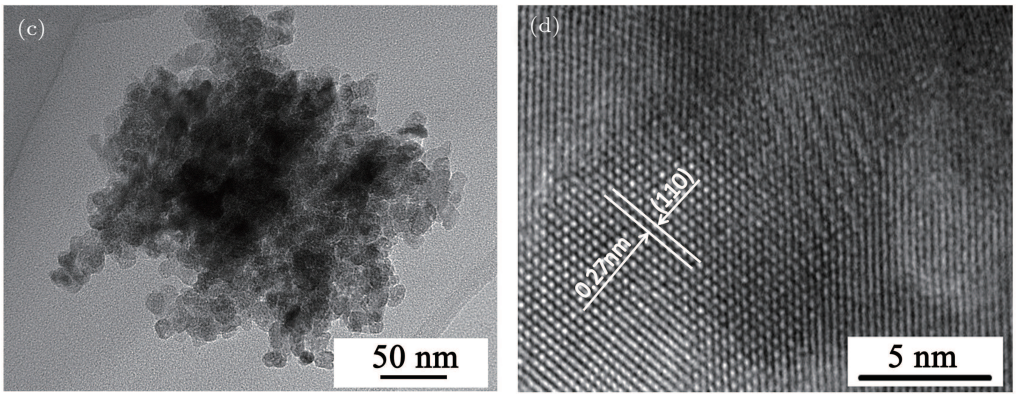


Fig. 2. (color online) (a) XRD patterns of STO/LaNb–STO powders, (b) EDS/TEM, (c) TEM image, and (d) high resolution TEM image for STO/La10Nb20 powder.

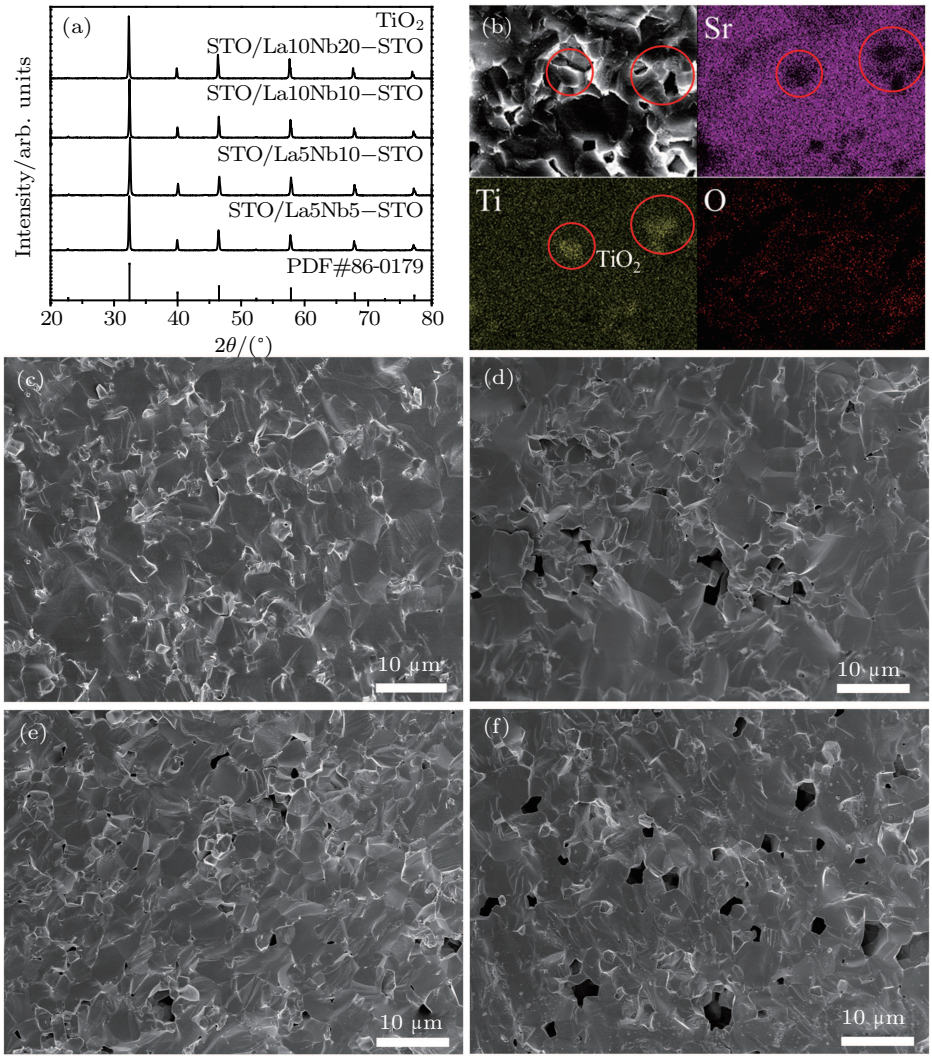


Fig. 3. (color online) (a) XRD patterns of STO/LaNb–STO disks; (b) EDS mapping for STO/La10Nb20–STO disk; SEM images for (c) STO/La5Nb5–STO, (d) STO/La5Nb10–STO, (e) STO/La10Nb10–STO, and (f) STO/La10Nb20–STO.

The XRD patterns of disk samples are shown in Fig. 3(a). It can be seen that a small number of TiO_2 impurity peaks appear in the STO/La10Nb20–STO sample after sintering. A Ti-rich Sr-poor area has been observed from the EDS/SEM mapping image, as shown in Fig. 3(b). Both experimental facts indicate that a second phase of TiO_2 forms in the sintering process, which is in agreement with the results in a previous report.[31] Figures 3(c)–3(f) show the SEM images of microstructures of four composites. The grain size is about 5 μ–8 μm for all samples, while the grain size decreases with the increasing of doping concentration. Meanwhile, the porosities of samples also tend to increase with doping concentration increasing. The densities of samples decrease from a relatively higher value of 4.9 g/cm^3 for the STO/La5Nb5–STO sample

to 4.5 g/cm^3 for the STO/La10Nb20–STO sample, which may be related to the second phase of TiO_2 leading to the decrease of the density and the increase of the porosity. The occurring of the second phase and its related interface, and the increasing of grain boundary and porosity, would increase phonon scattering, which may be related to the reduction of thermal conductivity.

3.2. Analyses of thermoelectric properties

Figure 4 shows the temperature and doping concentration-dependent Seebeck coefficient (S), electrical conductivity (σ), and power factor (PF) for STO/LaNb–STO samples with different doping concentrations, respectively.

The Seebeck coefficients (Fig. 4(a)) for all samples are negative, indicating that the samples are n-type oxides. The Seebeck coefficient increases with increasing temperature, which is likely to be due to the decrease of the chemical potential for the sample with increasing temperature.[32] As can be seen from Fig. 4(b) the larger the doping concentration, the lower the value of $|S|$ is. The tendency is in good agreement with the equation of S for degenerate semiconductors,[29,33] as shown below.

$$S = -\frac{8\pi^2 k_B^2}{3eh^2} m^* T \left(\frac{\pi}{3n}\right)^{2/3}, \tag{1}$$

where k_B is the Boltzmann constant, e is the electronic charge, and n is the electron concentration. The Seebeck coefficient is inversely proportional to the total carrier concentration. It also indicates that the carrier concentration increases with the increase of doping concentration.[33]

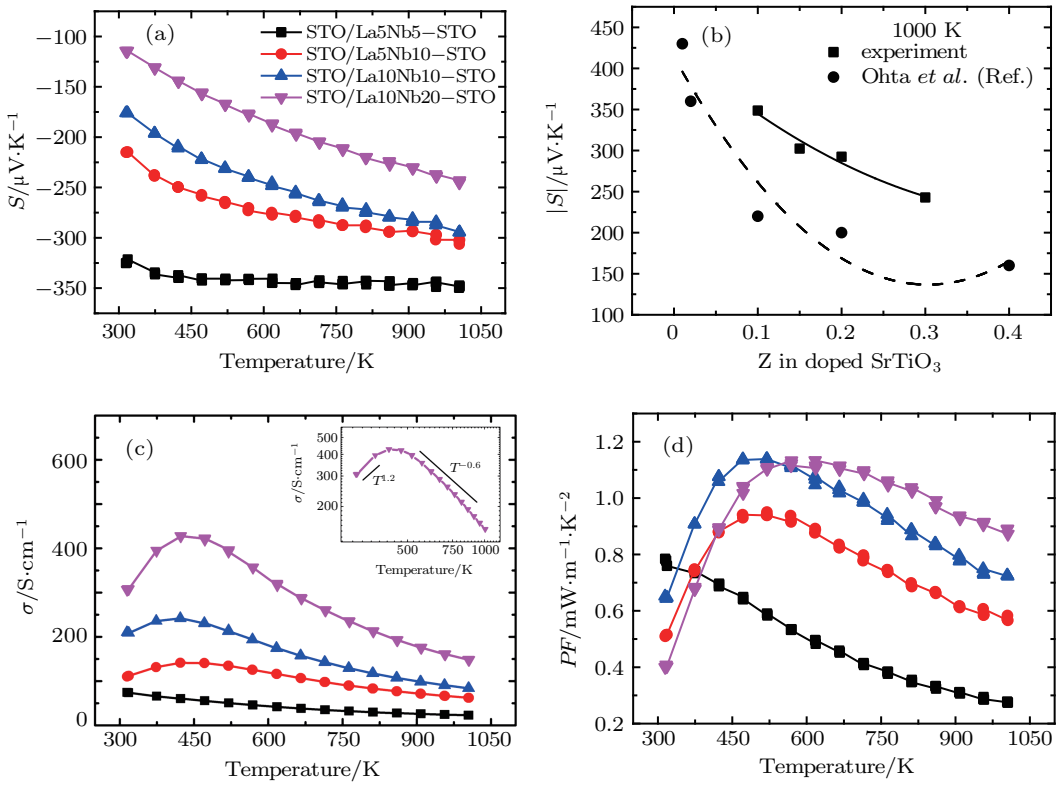


Fig. 4. (color online) Temperature-dependent (a) Seebeck coefficient, (c) electrical conductivity, and (d) power factor; (b) doping concentration-dependent Seebeck coefficient.

The Seebeck coefficient of the STO/La5Nb5–STO sample has a maximum value of 350 μV/K at 1000 K, that is the largest value obtained in the present study. The value is higher than the data reported previously for the same doping concentration,[34] which may suggest that the composites having more complex microstructure can cause interface effects such as energy filtering effect,[35] etc. The electrical conductivity (Fig. 4(c)) first increases and then decreases with temperature increasing (except for STO/La5Nb5–STO which decreases monotonically) throughout the testing period, which is consistent with the property of a semiconductor. The figure also reveals that the electrical conductivity increases with doping concentration increasing, and its maximum value is 420 S·cm^{-1} in the STO/La10Nb20–STO sample. In the case of a degenerated STO semiconductor, the carrier concentration is constant in a temperature range from room temperature to 1000 K.[29] Therefore, the temperature dependence of electrical conductivity is mainly affected by the carrier mobility according to the equation $\sigma = en\mu$ (where e is the electron charge, n is the election concentration, and μ is the carrier mobility). As shown in the inset of Fig. 4(c), at low temperature the electrical conductivity increases proportionally to $T^{1.2}$ approximately, especially in high doping concentration, indicating a main contribution from ionized impurity scattering.

The decrease of electrical conductivity is proportional nearly to $T^{-0.6}$ at high temperatures, which implies a dominant scattering by acoustic phonons.[29,36] The power factor (Fig. 4(d)) of the sample is calculated from the equation $PF = S^2\sigma$. It can be seen that the power factor decreases slowly after rapidly rising (except for STO/La5Nb5–STO) with temperature increasing. The tendency is consistent with that of electrical conductivity: as the doping concentration increases, the peak value of power factor shifts to higher temperature. Although the maximum power factor of 1.14 mW·m^{-1}·K^{-2} is obtained in the STO/La10Nb10–STO sample at 520 K, from the high temperature above 570 K, the power factor increases with doping concentration increasing. These facts indicate the dominant contribution of electrical conductivity to the increase of PF.

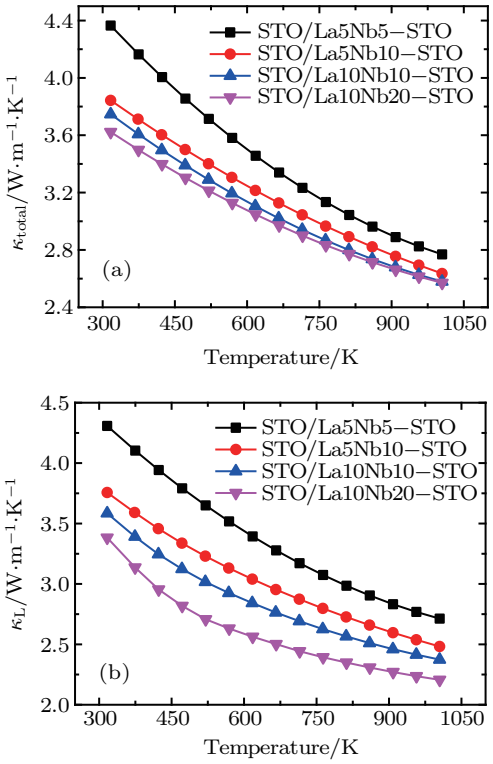


Fig. 5. (color online) Temperature-dependent (a) total thermal conductivities and (b) lattice thermal conductivities.

The total thermal conductivity is composed of lattice thermal conductivity (κ_L) and electronic thermal conductivity (κ_e), $\kappa = \kappa_L + \kappa_e$. The electronic thermal conductivity is calculated from the equation $\kappa_e = LT\sigma$ where L is the Lorenz number (2.44×10^{-8} V^2·K^{-2}). The total thermal conductivity and the lattice thermal conductivity are shown in Fig. 5. Both of them decrease gradually with the increasing of temperature. At high temperatures, the difference in the total thermal conductivity among samples becomes small, suggesting a dominant phonon scattering by the Umklapp process.[37] However, with the increase of doping concentration, the lattice thermal conductivity decreases, which may be related to some other reasons of phonon scattering by the interface, defect, porosity, ionized impurity, lattice distortion, etc., as indicated in the above-mentioned microstructure analysis. The thermal conductivities of both STO/La10Nb10–STO and STO/La10Nb20–STO samples decrease to 2.57 W·m^{-1}·K^{-1} at 1000 K, which is lower than that of mono phase STO bulk material.[31]

Finally, the thermoelectric figure-of-merit zT (Fig. 6) is calculated from the equation $zT = S^2\sigma T/\kappa$. With high PF and low thermal conductivity, a maximum zT value of 0.35 is obtained in the STO/La10Nb20–STO sample at 1000 K, and the value is relatively high compared with those reported previously.

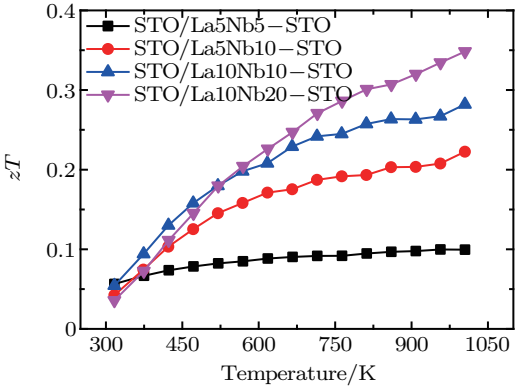


Fig. 6. (color online) Temperature-dependent zTs.

4. Conclusions

We have synthesized $SrTiO_3$/LaNb–$SrTiO_3$ composites with different doping levels by using a combination of hydrothermal method and a promising sintering method. A high $zT = 0.35$ at 1000 K is realized on an STO/La10Nb20–STO sample. With doping concentration increasing, the power factor increases, and the lattice thermal conductivity decreases dramatically. It appears that the high power factor arises from a reasonable balance point between the Seebeck coefficient and the electrical conductivity. The low thermal conductivity is likely to be related to stronger phonon scattering by the interface, defect, ionized impurity, and lattice distortion, which is attributed to the complex microstructure of $SrTiO_3$/LaNb–$SrTiO_3$ composite. It is fair to say that the thermoelectric properties could be further enhanced by using an appropriate microstructure and doping concentration.

References

[1] Tan G, Zhao L D and Kanatzidis M G 2016 *Chem. Rev.* **116** 12123
[2] Luo Y, Yang J, Li G, Liu M, Xiao Y, Fu L, Li W, Zhu P, Peng J, Gao S and Zhang J 2014 *Adv. Energy Mater.* **4** 1300599
[3] Luo Y, Yang J, Jiang Q, Li W, Zhang D, Zhou Z, Cheng Y, Ren Y and He X 2016 *Adv. Energy Mater.* **6** 1600007
[4] Zhao H, Cao B, Li S, Liu N, Shen J, Li S, Jian J, Gu L, Pei Y, Snyder G J, Ren Z and Chen X 2017 *Adv. Energy Mater.* **7** 1700446
[5] Pei Y, Tan G, Feng D, Zheng L, Tan Q, Xie X, Gong S, Chen Y, Li J F, He J, Kanatzidis M G and Zhao L D 2017 *Adv. Energy Mater.* **7** 1601450
[6] Fu L, Yang J, Peng J, Jiang Q, Xiao Y, Luo Y, Zhang D, Zhou Z, Zhang M, Cheng Y and Cheng F 2015 *J. Mater. Chem. A* **3** 1010

[7] Luo Y, Yang J, Liu M, Xiao Y, Fu L, Li W, Zhang D, Zhang M and Cheng Y 2015 *J. Mater. Chem. A* **3** 1251

[8] Zhao L D, Tan G, Hao S, He J, Pei Y, Chi H, Wang H, Gong S, Xu H, Dravid V P, Uher C, Snyder G J, Wolverton C and Kanatzidis M G 2016 *Science* **351** 141

[9] Liu W, Yin K, Zhang Q, Uher C and Tang X 2017 *Natl. Sci. Rev.* **4** 611

[10] Gibbs Z M, Ricci F, Li G, Zhu H, Persson K, Ceder G, Hautier G, Jain A and Snyder G J 2017 *NPJ Comp. Mater.* **3**

[11] Zhao W, Liu Z, Wei P, Zhang Q, Zhu W, Su X, Tang X, Yang J, Liu Y, Shi J, Chao Y, Lin S and Pei Y 2017 *Nat. Nanotechnol.* **12** 55

[12] Zhao W, Liu Z, Sun Z, Zhang Q, Wei P, Mu X, Zhou H, Li C, Ma S, He D, Ji P, Zhu W, Nie X, Su X, Tang X, Shen B, Dong X, Yang J, Liu Y and Shi J 2017 *Nature* **549** 247

[13] Sangwook Lee K H, Fan Yang, Jiawang Hong, Changhyun Ko, Joonki Suh, Kai Liu, Kevin Wang, Jeffrey J Urban, Xiang Zhang, Chris Dames, Sean A Hartnoll, Olivier Delaire and Junqiao Wu 2017 *Science* **355** 371

[14] Nunna R, Qiu P, Yin M, Chen H, Hanus R, Song Q, Zhang T, Chou M Y, Agne M T, He J, Snyder G J, Shi X and Chen L 2017 *Energ. Environ. Sci.* **10** 1928

[15] Cao B, Jian J, Ge B, Li S, Wang H, Liu J and Zhao H 2017 *Chin. Phys. B* **26** 017202

[16] Wang N, Li H, Ba Y, Wang Y, Wan C, Fujinami K and Koumoto K 2010 *J. Electron. Mater.* **39** 1777

[17] Wang N, He H, Ba Y, Wan C and Koumoto K 2010 *J. Ceram. Soc. Jpn.* **118** 1098

[18] Wang Y, Zhang X, Shen L, Bao N, Wan C, Park N H, Koumoto K and Gupta A 2013 *Journal of Power Sources* **241** 255

[19] Zhang L, Tosho T, Okinaka N and Akiyama T 2007 *Mater. Trans.* **48** 1079

[20] Kumar S R, Barasheed A Z and Alshareef H N 2013 *ACS Appl. Mater. Interfaces* **5** 7268

[21] Yu C, Scullin M L, Huijben M, Ramesh R and Majumdar A 2008 *Appl. Phys. Lett.* **92** 191911

[22] Kovalevsky A V, Aguirre M H, Populoh S, Patrício S G, Ferreira N M, Mikhalev S M, Fagg D P, Weidenkaff A and Frade J R 2017 *J. Mater. Chem. A* **5** 3909

[23] Zhang G, Wang W and Li X 2008 *Adv. Mater.* **20** 3654

[24] Dawson J A and Tanaka I 2014 *J. Phys. Chem. C* **118** 25765

[25] Maria Ibáñez R Z, Stéphane Gorsse, Jiandong Fan, Silvia Ortega, Doris Cadavid, Joan Ramon Morante, Jordi Arbio and Andreu Cabot 2013 *ASC Nano* **7** 2573

[26] Park N H, Akamatsu T, Itoh T, Izu N and Shin W 2015 *Materials* **8** 3992

[27] Marcus Scheele N O, Igor Veremchuk, Sven-Ole Peters, Alexander Littig, Andreas Kornowski, Christian Klinke and Horst Weller 2011 *ASC Nano* **5** 8541

[28] Chen X, Wang Y C and Ma Y M 2010 *J. Phys. Chem. C* **114** 9096

[29] Wang J, Zhang B Y, Kang H J, Li Y, Yaer X, Li J F, Tan Q, Zhang S, Fan G H, Liu C Y, Miao L, Nan D, Wang T M and Zhao L D 2017 *Nano Energy* **35** 387

[30] Shannon R D 1976 *Acta Crystallogr. A* **32** 751

[31] Zhang B, Wang J, Zou T, Zhang S, Yaer X, Ding N, Liu C, Miao L, Li Y and Wu Y 2015 *J. Mater. Chem. C* **3** 11406

[32] Shingo Ohta H O and Kunihito Koumoto 2006 *J. Ceram. Soc. Jpn.* **114** 102

[33] Cutler M, Leavy J F and Fitzpatrick R L 1964 *Phys. Rev.* **133** A1143

[34] Ohta S, Nomura T, Ohta H, Hirano M, Hosono H and Koumoto K 2005 *Appl. Phys. Lett.* **87** 092108

[35] Ou C, Hou J, Wei TR, Jiang B, Jiao S, Li J F and Zhu H 2015 *NPG Asia Mater.* **7** e182

[36] Shen J, Zhang X, Lin S, Li J, Chen Z, Li W and Pei Y 2016 *J. Mater. Chem. A* **4** 15464

[37] Li W, Lin S, Zhang X, Chen Z, Xu X and Pei Y 2016 *Chem. Mater.* **28** 6227